
Assessment and prediction of forest health risk (FHR) for effective planning and management in mining stressed forest area

7.1	Overview	113
7.2	Data sources	113
7.3	Field observation	114
7.4	Data pre-processing	114
7.5	Causative factors of forest health risk	115
7.5.1	Climate factors	115
7.5.2	Geomorphologic factors	115
7.5.3	Forestry factors	116
7.5.4	Topographic factors	116
7.5.5	Environmental factors	117
7.5.6	Anthropogenic factors	117
7.6	Methodology	117
7.6.1	AHP (Analytical hierarchy process) model	117
7.6.2	Forest health risk (FHR) assessment and prediction in mines	120
7.6.3	Sensitivity Analysis	120
7.6.4	Statistical correlation of sensitive parameters	121
7.6.5	Comparison and validation	121
7.6.6	Relationship between FHR, distance from mines with foliar d	121
7.7	Results and Discussion	122
7.7.1	Present and predicted factors	122
7.7.2	FHR assessment and prediction in mines surrounding sites	124
7.7.3	Identification of sensitive factors	126
7.7.4	Correlation of sensitive factors	127
7.7.5	Comparison and validation	128
7.7.6	Relationship between FHR, distances from mines with foliar	129
7.7.7	Discussion	130
7.8	Summary	132

This Chapter has originally been published as: **Kayet, N., Pathak, K., Chakrabarty, A., Kumar, S., Chowdary, V. M., & Singh, C. P. (2020)**. Risk assessment and prediction of forest health for effective geo-environmental planning and monitoring of mining affected forest area in hilltop region. **Geocarto International (Taylor & Francis)**, SCI, Impact Factor-4.89

7.1 Overview

Due to climate change and increased anthropogenic activities, the forests are likely to face the risk to health. In the Saranda forest, forest health gets severely affected by iron ore mining activities, climate change, and air pollutions over the last 35 years, and it continues to get affected in the future too. So, it is essential to monitor forest health risk (FHR) in surrounding mining affected forest region.

7.2 Data sources

For the FHR study, satellite data (Hyperion, Landsat, Quickbird, Cartosat-1-DEM, and Sentinel-1) were collected from the various sources (Earth Explorer, Google Earth, Sentinel hub, and Bhuvan). We studied the FHR for the years present and predicted due to the data's availability, precision, and accuracy. From the years 1980 to the present (in 1 km grid), climate data were downloaded from the NCEP (www.ncep.noaa.gov/) website for the present analysis. Using the RCP 4.5 model, climate data (in 1km) were obtained from the IPCC (www.ipcc.ch) website from 2000 to 2050 for predicted analysis. Collected mean max and mini temperature, rainfall, and solar radiation data were converted to a spatial raster grid using IDW (Inverse distance weighting) method in ArcGIS software (developed by ESRI) for predicted years. LULC (land use and land cover) maps were prepared using the MOLUSCE (modules for land use change simulations) model in QGIS software's plugin (developed by nest GIS and Asia air survey) for predicted years. Deforestation susceptibility (DS) data for the same predicted years were also prepared using a multi-criterion based AHP model. The soil, lithology, and geomorphology data were collected from various source NBSS (www.nbsslup.in), GSI (www.gsi.gov.in), and Bhuvan (www.bhuvan.nrsc.gov.in) and prepared for present years. Forest density data were collected from the Chaibasa forest department of Jharkhand. From work done by Kayet et al. (2019 a&b), forest health, foliar dust, plant diversity, and tree species data were prepared for the present year. From the Google Earth image, the deforestation map (present) was greatedened using time-series data. Using the Cartosat-1 stereo image, DEM (digital elevation model) was prepared to evaluate altitude and slope data for the present year. LST (land surface temperature), hot spot, NDVI, and drought data were generated by different models based on satellite imagery (Landsat 8 OLI) and climate data. The distance from settlements, roads, and mines data were performed from Google Earth's image and Toposheet. In the study region, tree's spectral, foliar dust, and precise locations GPS (global positioning system) data for forest healthy

and unhealthy data were collected by different instruments for validation purposes. Data source details shown in (Appendix.3).

7.3 Field observation

The field surveys were conducted into dry season in the Saranda forest. We have recorded sixty tree's leaf spectra (healthy and unhealthy trees) using a spectroradiometer during the time of field survey. These spectra were used for accuracy assessment of FHR. Also, we have collected foliar dust concentration using PCE-RCM 05 (dust instrument) and collected the GPS (Garmin) location points to validate FHR results. During the field survey, we observed a clear negative relationship between FHR and mining.

7.4 Data pre-processing

Satellite data were pre-processed by scientific methods (geometric, radiometric, atmospheric, and terrain correction) in the image processing software (ENVI-developed by Harris geospatial solutions). We have used the FLAASH (fast line-of-sight atmospheric analysis of the hypercubes) model for atmospheric correction of satellite imagery (Anderson et al., 2002). A total of sixty spectra corresponding to different tree species were recorded, and the mean spectra of each tree species were used to analyze forest health conditions. Pre-processing field spectra consisted of temperature drift correction, water absorption, noise bands removal, and spectral smoothing using ASD FieldSpec software. The average spectra of tree species were calculated after spectral smoothing. These average spectres were used for spectral library development in ENVI and applied to classify forest health conditions (Kayet et al., 2019a).

Many researchers worked on RCP 4.5, 6.0, and 8.5 models for predictive analysis (Raju et al., 2017; Chakraborty et al. 2019). It has been observed from the literature review that the result obtained by the RCP 4.5 model shows a better fit for the Indian climate condition, so we have used this model-based climate data for this analysis. Max & mini temperature, solar radiation, and rainfall data were bias-corrected by LS (linear scaling) method and converted a regional scale using the downscaling method (Raju et al., 2017; Fang et al., 2015). Cartosat-1 DEM data was corrected through the C-correction method (Kobayashi & Sanga, 2009) in the image processing tool of LPS software (developer by hexagon geospatial) based on DGPS (differential global positioning system) survey points. The geomorphic (soil, geomorphology, and lithology) and forest density factors were rectified from collected maps (toposheet) using the rectification tool of Arcmap. The

anthropogenic factors (distance from mines, roads, & settlements) were digitized (polygons) from the Google earth image as well as toposheet and corrected the topological error in the topology tool of Arcmap. All pre-processed datasets were re-projected into the UTM (45° north) coordinate system with WGS-84 data and converted to a raster grid cell (30m×30m) multi-criteria model based FHR analysis.

7.5 Causative factors of forest health risk

Many causative factors such as climate (max & min temperature, rainfall, wind speed and drought), geomorphology (soil, geology, geomorphology and LULC), forestry (forest health, forest density, tree species, plant diversity, NDVI & deforestation), topography (slope & altitude), environmental (LST, hot spot, & foliar dust), and anthropogenic activities (distance from mines, roads, and settlements) are affected the forest health (Trumbore & Hartmann, 2015; Gauthier et al., 2015; Saha et al., 2020). We have also used predicted factors (max & mini temperature, rainfall, solar radiation, LULC, and deforestation susceptibility) for prediction FHR using a multi-criteria-based AHP model. The details of the present and predicted factors are shown below.

7.5.1 Climate factors

The climate factors (min & max temperature, rainfall, and wind speed) are the primary causative factors of FHR. Due to climate factors, the FHR rate is increasing day by day. The climate factors affect forest growth and productivity, which in turn affects risk to forest health (Holeksa et al., 2017; Ramsfield et al., 2016). The pre-processed rainfall (annual average), min & max temperature, and wind speed (monthly average) non-spatial data for the present year were converted to spatial grid format (raster) using the IDW tool in Arcmap. Also, predicted climate data (average min & max temperature, rainfall, and solar radiation) for the temporal domains (2030 & 2050) were generated from the RCP 4.5 climate model and converted to spatial raster format using Arcmap.

Drought directly affects trees by growth as well as causing injury or death. Also, it indirectly affects forest health by increasing insect pests, wildfire, and disease (Klos et al., 2009; Jactel et al., 2012). Some factors are directly and indirectly linked to drought. For drought analysis, some researchers had used eight indices likes rainfall, temperature, NDVI, LST, SMI (soil moisture index), SAVI (soil-adjusted vegetation index), VCI(vegetation condition Index), and VTCI (vegetation temperature condition index) based on the multi-criteria analysis in GIS platform (Rahman et al., 2016; Belal et al.,

2014; Schwarz et al., 2020). We have used climate and satellite imagery data, and the aforesaid mentioned indices were calculated based on the raster calculator tool in Arcmap. These indices have been used to prepare drought raster data for FHR analysis.

7.5.2 Geomorphological factors

Soil is an indicator of forest health. Soil type and properties data are used to determine the forest's stress level and health, and it may be one factor used to assess the risk of health (Pritchett, 1980; Kopackova et al., 2015). Tree species community, its distribution, and their health depend on the soil, lithology, LULC and geomorphological condition (Fayolle et al., 2012; Ozcelik, 2008; Trumbore et al., 2015). Soil, geology, and geomorphology data were digitized and converted to spatial raster grid format for FHR analysis using Arcmap.

LULC data were generated from Landsat imagery using the SVM algorithm. We had classified LULC into seven classes (dense forest, moderate forest, open forest, agricultural land, waterbody, built-up land, and wasteland). For predicted LULC, we had used the MOLUSCE plugin in QGIS software. MOLUSCE well simulates the changes in land-use between different periods (Gismondi et al., 2014). The ANN (artificial neural network) algorithm of the MOLUSCE plugin was applied to simulate land-use change for the years 2030 and 2050. The methodology adopted for LULC simulation from the study of Mohammadi et al. (2018).

7.5.3 Forestry factors

Tree species, diversity, and distribution are directly related to the risk of forest health (Bussotti et al., 2018). In the prior study (Kayet et al., 2019 a & b; Kayet et al., 2020), forest health, tree species, and plant diversity factors were generated from satellite imagery (Hyperion) and tree spectral data based on the spectroradiometer instrument. Forest density data were rectified and digitized for various forest features using the Arcmap tool and converted to spatial raster grid format. NDVI generated high and low values (0 to 1) are indicated healthy and unhealthy vegetation (Tuominen et al., 2009). NDVI raster data was generated from the Red and NIR bands of Landsat 8 OLI imagery using raster calculator tool in Arcmap. Deforestation is one of the significant factors for FHR analysis. Long term deforestation results in unhealthy or degraded forests (Chakravarty et al., 2012).

For predicted deforestation susceptibility, we used eighteen of the present (aspect, elevation, geology, soil, LST, LULC, hot spot, drought, geomorphology, min & max temperature, forest density, NDVI, precipitation, slope radiation, distance from mines, roads, and settlements) and five predicted causative factors (min & max temperature, precipitation, slope radiation, and LULC) from future time domain for simulated deforestation susceptibility (DS) for the years present and predicted (2030 and 2050) using multi-criteria based models. The methodology of deforestation susceptibility was adopted by Kayet et al., (2020) paper.

7.5.4 Topographic factors

Topographical parameters (elevation, slope, and aspect) are critical factors responsible for the risk of forest health or deforestation (Kumar et al., 2015). The low slope or moderate altitude conditions are suitable for the healthy forest, and high slope and altitude are suitable for unhealthy forests (Zirlewagen et al., 2007). From the DEM image altitude and slope, data were generated and classified into five different classes of spatial analysis tools in ArcGIS. The study area poses the elevation variation of 220 to 860 meters and slope variation of 7 to 38-degrees.

7.5.5 Environmental factors

Forest health conditions are too affected by the highest surface temperature or hotspot area. There is a negative relationship between surface temperature and forest health (Rogan et al., 2013; Fei, 2010; Wolff et al., 2018). In the prior study (Kayet et al. 2016. a&b), LST and hot spot raster data were also generated from satellite imagery (Landsat-8 OLI) and other data with different models using the image processing tool of ENVI. Mining borne dust affects plants' growth, the forest's productivity, and changes the plant community structure (Tuominen et al., 2008). In the prior study (Kayet et al. 2019.b), narrow banded VIs (vegetation indices) tool based foliar dust raster data were generated from Hyperion satellite imagery and ground-based dust spectra data. The foliar dust concentration (g/m²) of the study area varies from 4 g/m² to 84 g/m². The area surrounding the mines, dump area, and transport sites exhibited higher foliar dust concentration.

7.5.6 Anthropogenic factors

The presence of human interference near mines leads to the development of roadways, house construction, transportation, and other allied activities that also impose a risk to forest health (Cueva et al., 2019; Chomitz and Gray., 1999). The anthropogenic activities (distance from mines, roads, and settlements) vector data were generated by Google earth imagery and Toposheet. Using the Arcmap digitization tool, mines, roads network, and settlements areas were demarcated (visual interpretation) and converted to spatial raster grid format using the IDW interpolation method.

7.6 Methodology

7.6.1 Application of AHP (Analytical hierarchy process) model

AHP model is useful for multi-criterion overlay weighted analysis. Multi criterion decision analysis (MDCA) fits well for the principles of AHP (Gigovic et al., 2017). Some researchers have used AHP based multi-criteria model for present and future simulation of the forest fire, environmental vulnerability and land-use suitability were analysed in a GIS platform based on causative factors (Chakraborty et al. 2019; Sahoo et al., 2019). That is why we had used AHP method for the assessment and prediction of FHR in our study area. The following Eq.7.1 calculates the FHR (Dhar et al., 2015).

$$FHR_{px,py} = \sum_{i=1}^{N_F} w_i \left[\sum_{k=1}^{N_{SF}^i} w_i^k \chi_{A_i^k} \left(C_{px,py}^v \Big|_i \right) \right] \quad (\text{Eq-7.1})$$

where index i represents causative factors attribute and k represents causative factor sub- attribute classes; N_F denotes the overall number of factor attributes; N_{SF}^i denotes the number of sub-classes attributes for i th attribute; w_i^k denotes the FHR value for k th sub-classes attribute and i th attribute; $C_{px,py}^v \Big|_i$ denotes the class value for (px, py) cell of i th attribute; A_i^k represents the interval of sub-classes attribute; $\chi_{A_i^k}$ represents indicator function for the k th sub-classes attribute of i th attribute and defined as (Eq.7.2). Eq.7.2 is the description of part of Eq-7.1.

$$\chi_{A_i^k} \left(c_{px,py}^v \right) = \begin{cases} 1 & \text{if } C_{px,py}^v \Big|_i \in A_i^k, \\ 0 & \text{if } C_{px,py}^v \Big|_i \notin A_i^k. \end{cases} \quad (\text{Eq.7.2})$$

AHP model can be useful for FHR assessment and prediction of relative-weight (w_i) and normalized-weight (w_i^k). The following steps are used for the calculation of weights and consistency ratios (C.R).

Step-1 Development of judgment matrices (A) by pair wise comparison

AHP is constructed by pairwise comparison matrices (PCM). In these matrices, each factor is related to another factor and assigned by relative dominance value from 0 to 9 (Dai & Blackhurst, 2012). For each factor of hierarchy structure, it is linked to all factors. These factors are compared and calculated relative weights for each factor based on PCM (Eq.7.3).

$$A = \begin{bmatrix} 1 & \frac{P_1}{P_2} & \dots & \frac{P_1}{P_n} \\ \frac{P_2}{P_1} & 1 & \dots & \frac{P_2}{P_n} \\ \dots & \dots & \dots & \dots \\ \frac{P_n}{P_1} & \frac{P_n}{P_2} & \dots & 1 \end{bmatrix} \quad (\text{Eq.7.3})$$

Where, A indicates the PCM; P_1, P_2 denotes the weight of element 1 and 2; P_n indicates the weight of element n.

Step-2 Calculation of relative weight (w_k)

The relative weights (w_k) is calculated for each factor in PCM (Eq.7.4).

$$W_k = GM_k / \sum_{m \in F} GM_m \quad (\text{Eq.7.4})$$

Where, the geometric mean of the kth row of judgment matrix is calculated as $GM_k = \sqrt[N_F]{a_{k1} a_{k2} \dots a_{kN_F}}$, N_F is the total number of features.

Step-3 Calculation of consistency ratio (C.R)

For strength assessment of each factor is used consistency ratio. CR is calculated by the following equation (Eq.7.5).

$$CR = \frac{CI}{RI} \quad (\text{Eq.7.5})$$

The CR is acquired by comparing CI (consistency index) with the appropriate values in which each is an average consistency index using the scale (1/9, 1/8, 1/7, 1/6, 5...1) (Kwiesielewicz et al., 2004). For a randomly generated reciprocal matrix, the CI shall be called to the RI (random index). The CI of the pairing matrix ensures that the judgment of the decision-maker is consistent.

Step-4 Calculation of consistency index (CI)

CI is calculated by Eq.7.6.

$$C.I. = \frac{\lambda_{\max} - N_F}{N_F - 1} \quad (\text{Eq.7.6})$$

Step-5 Calculation of final normalized-weight (w_i^S)

The normalized-weight (w_i^S) of decision elements is combined with an overall rating. The last step in AHP is relative weight of decision elements collectively used to obtain overall rating for alternatives by Eq.7.7.

$$w_i^s = \sum_{j=1}^{j=m} w_{ij}^s w_j^a, i = 1, \dots, n \quad (\text{Eq.7.7})$$

Where, w_i^S denotes the total weight of site i, w_{ij}^S denotes the weight of alternative i related to attribute (map layer) the attribute j, w_j^a indicated the weight of the attribute, and n represents the number of site. The same procedure should be followed for w_i^k calculation. The final normalized-weight values thus obtained were used for forest health risk (FHR) assessment and prediction maps from the abovementioned procedure.

7.6.2 Forest health risk (FHR) assessment and prediction in mines surrounding sites

AHP model combined with different causative factors of FHR and analyzed by the GIS weighted overlay method was used to generate FHR maps in the temporal domain (present and future). Based on literature reviews (Sahana et al., 2018; Saha et al.,

2020) FHR map is classified into five classes (very high, very, moderate, low, and very low). In this work, we have focused on the results of FHR at the surrounding two mines (Kiriburu and Meghahatuburu) sites. However, the overall flowchart for FHR assessment and prediction is shown in Figure.7.1.

7.6.3 Sensitivity analysis

Sensitivity analysis identifies the factors that affect the risk assessment more, based on numerical models (Dhar et al., 2015; Sahoo et al., 2019). This analysis is used to develop or apply environmental models to improve the understanding of parameter behaviors and impact and interactions of model parameters (Mair et al., 2012). In this work, a sensitivity analysis was done by all FHR related causative factors and identified the factors that have a higher impact on FHR. Eq.7.8 can calculate sensitivity analysis.

$$MS_i^j = \frac{s_{-i}^j - s_f^j}{s_f^j} \times 100(\%) \quad (\text{Eq.7.8})$$

Where, i attribute's subscripts, j is the AHP based output class superscript. MS_i^j represents the FHR class alteration (+/-) of the study area due to the absence of ith parameter. Subsequent, s_{-i}^j is the jth type of FHR class due to exclusion of ith component, s_f^j stand for the jth type of FHR class using all factors.

7.6.4 Statistical correlation of sensitive parameters

In this study, the Pearson correlation method has been used to know the relationship between FHR and sensitive factors. This correlation coefficient or the bivariate correlation measures the linear correlation between independent (IDV) and dependent (DV) variables (Benesty et al, 2009). Its value range between +1 to -1, where +1 indicates a positive linear correlation, and -1 indicates a negative linear correlation, and 0 denotes no correlation (Hamby, 1994) (E.q.7.9).

$$r = \frac{\sum_{j=1}^n (x_{ij} - \bar{x}_i)(y_j - \bar{y})}{\left[\sum_{j=1}^n (x_{ij} - \bar{x}_i)^2 \sum_{j=1}^n (y_j - \bar{y})^2 \right]^{0.5}} \quad (\text{Eq.7.9})$$

Where, n is the sample size, x_i, y_i , and x_{ij} indicate the individual sample point which is indexed with i and $\bar{x} = \frac{1}{n} \sum_{j=1}^n x_i$ is the sample mean, which corresponds to \bar{y} .

7.6.5 Comparison and validation

The ROC curve is a beneficial tool for quality comparison, probabilistic, & prediction determination (Swets, 1988; Park et al., 2004). This curve also combines the sensitivity and specificity error matrix. An AUC (area under the curve) value (0.5 to 1 .0) of the ROC curve indicates a perfect match (Yesilnacar and Topal, 2005). Finally, the FHR assessment result has been validated by sixty field locations of healthy and unhealthy trees in the Saranda forest based on the ROC curve. ROC curve is given by Eq.7.10.

$$y = \sum_{i=1}^n (x_{i+1} - x_i)(y_{i+1} - y_i - y_i/2) \quad (\text{Eq.7.10})$$

Where, y denotes the area under the curve (AUC). & x indicates the 1-specificity (sensitivity).

Relationship between forest health risk, distance from mines with foliar dust concentration

Two primary iron ore mines (Kiriburu and Meghahataburu) are located in the study region, and these mines affect forest health as well as the ecosystem. We have tried to establish a relationship between the forest health risk (0 to 1 scale), distance from mines (meter), and foliar dust concentration (gm/m²) in the two mines buffer areas. The foliar dust concentration data were collected from the paper in the study region (Kayet et al., 2019.b). The distance of twenty sample points of FHR from mines has been calculated using ArcGIS software's measurement tool.

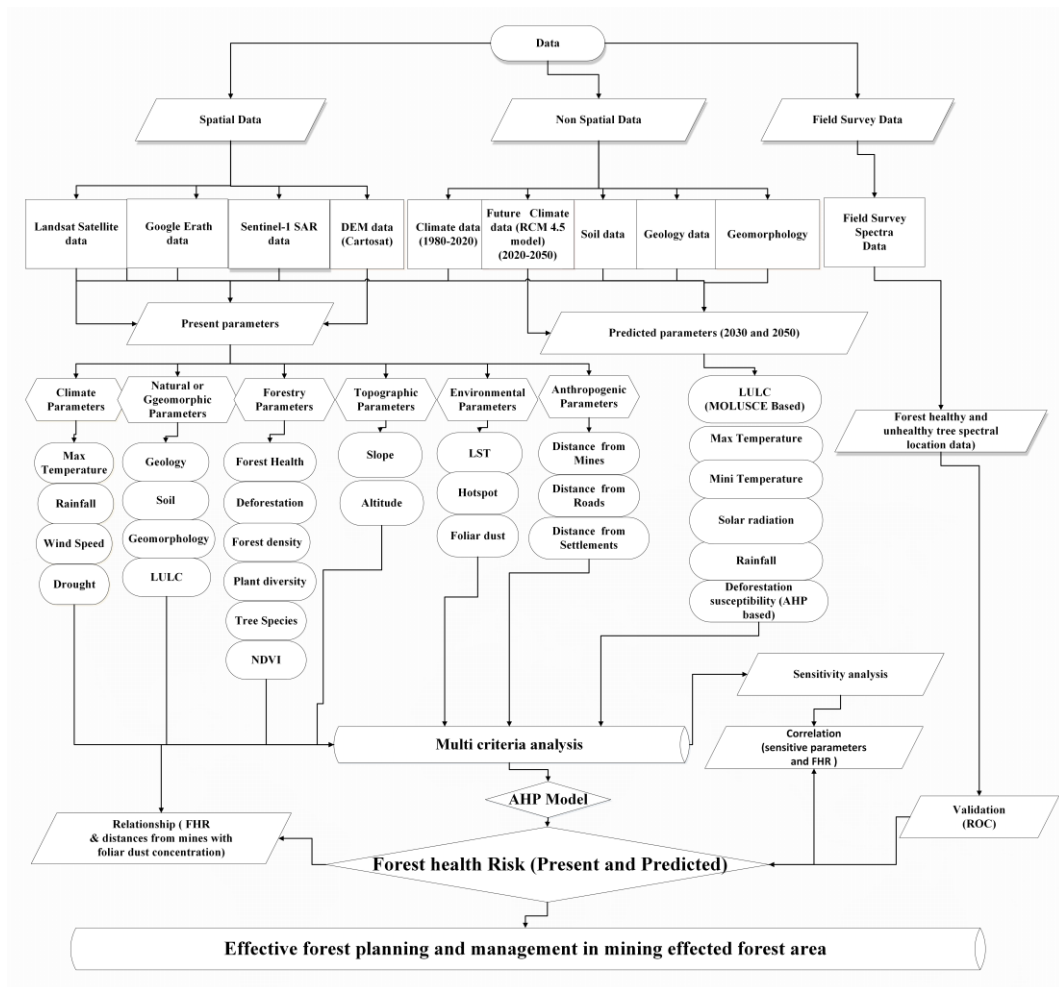


Figure.7.1: Overall flowchart of FHR assessment and prediction

7.7 Results and Discussion

7.7.1 Present and predicted factors

Since the study area was located in the mining field, it induces a lot of problems to forest health, which entails forest health monitoring. All the causative factors of forest health were classified and assigned sub weighted values based on the literature review, field experience, and specific study area (Appendix.4). Based on the trial & error approach, the numbers of classifying features have been considered to maximize the informative representation. The maps of twenty-eight (twenty present and six predicted) factors for the years present and predicted are shown in Figure.7.2 (a, &b

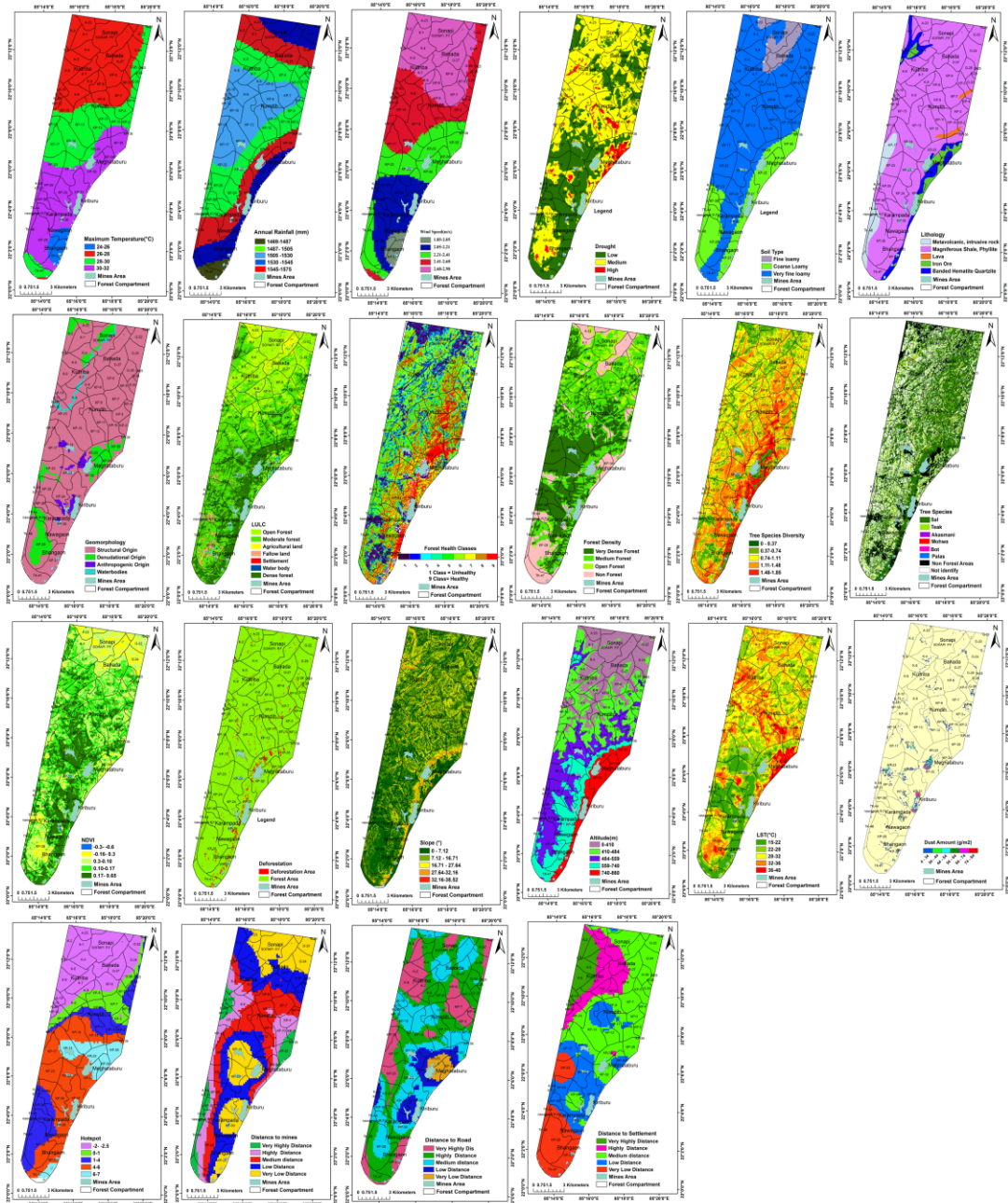


Figure 7.2.a: Present causative parameters of forest health

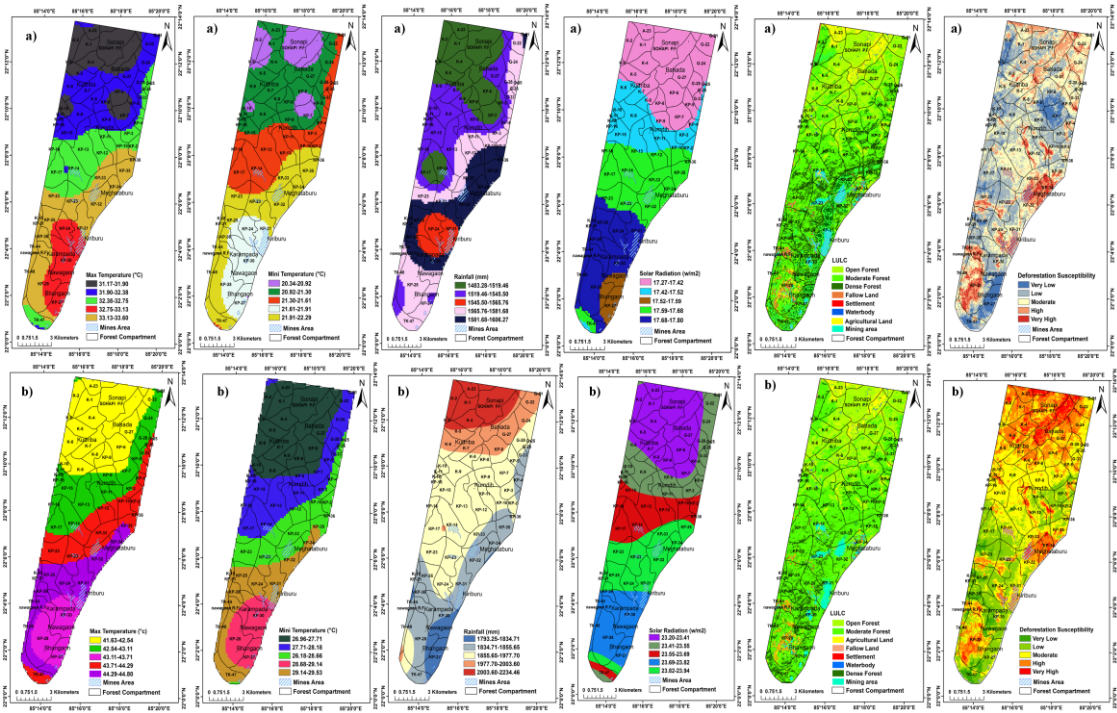


Figure 7.2.b: Predicted causative parameters of forest health (2030 (a) & 2050 (b))

7.7.2 Forest health risk assessment and prediction in mines surrounding sites

For the mining-affected forest area, FHR assessment as well as prediction in present and predicted time domain had been performed by twenty-eight causative factors using multi-criterion based AHP model in GIS framework. Final normalized-weighted results were calculated and integrated with all causative factors using the AHP model for FHR assessment and prediction (Table.7.1).

Table 7.1: Final normalized weighted of forest health causative parameters developed from AHP-based model

Features	T	R	WS	D	S	L	G	LU	FH	FD	TSD	TS	N	D	S	M	L	HS	FD	MD	RD	SD	Normalized weights
Temperature °C (T)	7/7	7/5	7/4	7/7	7/4	7/3	7/5	7/4	7/9	7/8	7/8	7/6	7/3	7/6	7/5	7/5	7/7	7/8	7/8	7/7	7/7	7/3	0.058
Rainfall (mm) (R)	5/7	5/5	5/4	5/7	5/4	5/3	5/5	5/4	5/9	5/8	5/8	5/6	5/3	5/6	5/5	5/5	5/7	5/8	5/8	5/7	5/7	5/3	0.031
Wind speed (m/s) (WS)	4/7	4/5	4/4	4/7	4/4	4/3	4/5	4/4	4/9	4/8	4/8	4/6	4/3	4/6	4/5	4/5	4/7	4/8	4/8	4/7	4/7	4/3	0.043
Drought (D)	7/7	7/5	7/4	7/7	7/4	7/3	7/5	7/4	7/9	7/8	7/8	7/6	7/3	7/6	7/5	7/5	7/7	7/8	7/8	7/7	7/7	7/3	0.058
Soil (S)	4/7	4/5	4/4	4/7	4/4	4/3	4/5	4/4	4/9	4/8	4/8	4/6	4/3	4/6	4/5	4/5	4/7	4/8	4/8	4/7	4/7	4/3	0.033
Lithology (L)	3/7	3/5	3/4	3/7	3/4	3/3	3/5	3/4	3/9	3/8	3/8	3/6	3/3	3/6	3/5	3/5	3/7	3/8	3/8	3/7	3/7	3/3	0.025
Geomorphology (G)	5/7	5/5	5/4	5/7	5/4	5/3	5/5	5/4	5/9	5/8	5/8	5/6	5/3	5/6	5/5	5/5	5/7	5/8	5/8	5/7	5/7	5/3	0.041
LULC (LU)	4/7	4/5	4/4	4/7	4/4	4/3	4/5	4/4	4/9	4/8	4/8	4/6	4/3	4/6	4/5	4/5	4/7	4/8	4/8	4/7	4/7	4/3	0.033
Forest health (FH)	9/7	9/5	9/4	9/7	9/4	9/3	9/5	9/4	9/9	9/8	9/8	9/6	9/3	9/6	9/5	9/5	9/7	9/8	9/8	9/7	9/7	9/3	0.075
Forest density (FD/T)	8/7	8/5	8/4	8/7	8/4	8/3	8/5	8/4	8/9	8/8	8/8	8/6	8/3	8/6	8/5	8/5	8/7	8/8	8/8	8/7	8/7	8/3	0.066

Plant diversity (PD)	8/7	8/5	8/4	8/7	8/4	8/3	8/5	8/4	8/9	8/8	8/8	8/6	8/3	8/6	8/5	8/5	8/7	8/8	8/8	8/7	8/7	8/3	0.066
Tree species (TS)	6/7	6/5	6/4	6/7	6/4	6/3	6/5	6/4	6/9	6/8	6/8	6/6	6/3	6/6	6/5	6/5	6/7	6/8	6/8	6/7	6/7	6/3	0.025
NDVI (N)	3/7	3/5	3/4	3/7	3/4	3/3	3/5	3/4	3/9	3/8	3/8	3/6	3/3	3/6	3/5	3/5	3/7	3/8	3/8	3/7	3/7	3/3	0.025
Deforestation (D)	6/7	6/5	6/4	6/7	6/4	6/3	6/5	6/4	6/9	6/8	6/8	6/6	6/3	6/6	6/5	6/5	6/7	6/8	6/8	6/7	6/7	6/3	0.025
Slope ° (S)	5/7	5/5	5/4	5/7	5/4	5/3	5/5	5/4	5/9	5/8	5/8	5/6	5/3	5/6	5/5	5/5	5/7	5/8	5/8	5/7	5/7	5/3	0.041
Altitude (m)	5/7	5/5	5/4	5/7	5/4	5/3	5/5	5/4	5/9	5/8	5/8	5/6	5/3	5/6	5/5	5/5	5/7	5/8	5/8	5/7	5/7	5/3	0.041
LST°C (L)	7/7	7/5	7/4	7/7	7/4	7/3	7/5	7/4	7/9	7/8	7/8	7/6	7/3	7/6	7/5	7/5	7/7	7/8	7/8	7/7	7/7	7/3	0.058
Hot spot (HS)	8/7	8/5	8/4	8/7	8/4	8/3	8/5	8/4	8/9	8/8	8/8	8/6	8/3	8/6	8/5	8/5	8/7	8/8	8/8	8/7	8/7	8/3	0.066

The FHR maps of the study area, for the years present and predicted are shown in Figure.7.3.

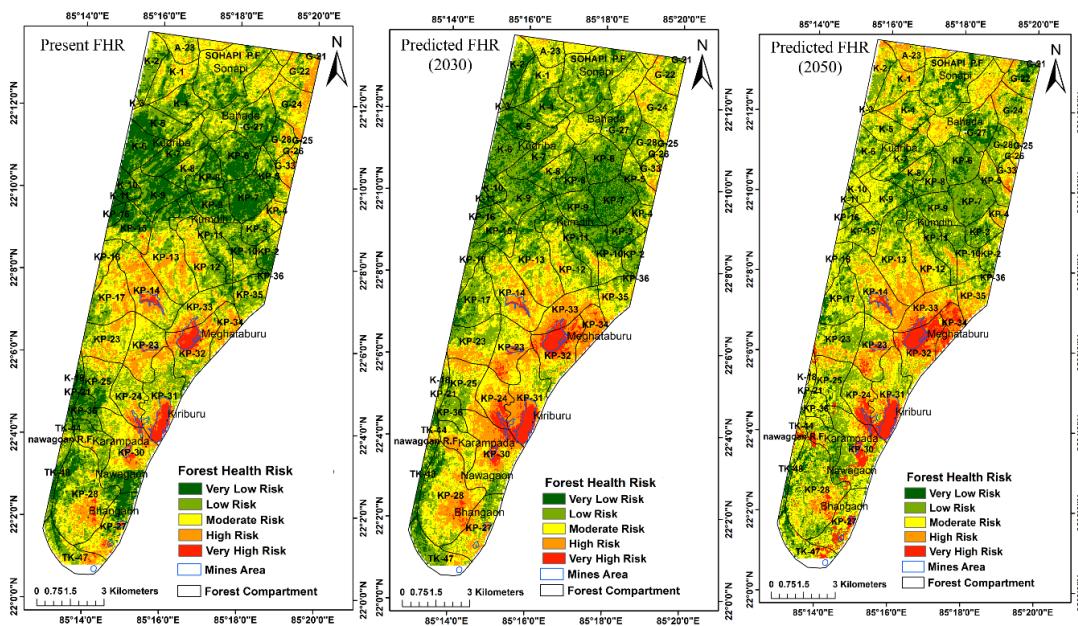


Figure.7.3: Comparative results of forest health risk (Present and predicted years)

The FHR maps thus prepared were classified into five different classes (namely very high, high, moderate, low, and very low). Table.7.2 shows how the FHR classes changes for the present and predicted years.

Table. 7.2: Zone-wise spatial coverage (%) of FHR results

Forest health risk (FHR) classes	Area (%)		
	Present	Predicted (2030)	Predicted (2050)
Very low risk	18.87	16.83	15.40
Low risk	32.68	33.78	33.62
Moderate risk	31.98	30.63	30.42
High risk	13.63	15.24	16.68
Very high risk	2.85	3.49	4.06

The magnified view of very high FHR compartments (surrounding two mines) are shown in Figure.7.4. The maps suggests that very high FHR zone is located near the Kiriburu and Meghahatuburu mines and its surrounding sites. The low FHR zone is situated in the upper and the lower hillsides of the study area.

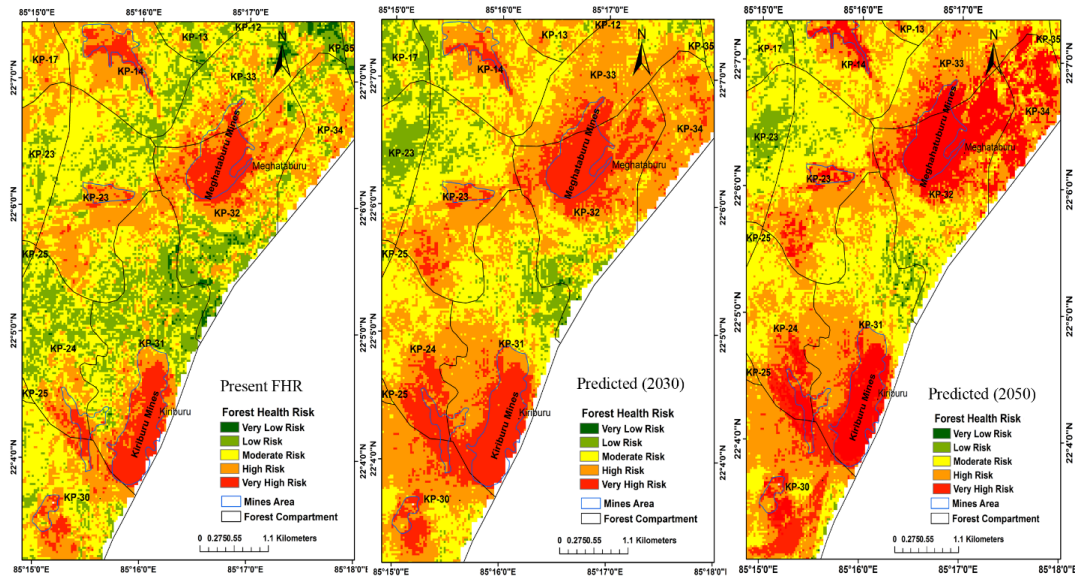


Figure.7.4: Magnified view of the comparative FHR results (Present and predicted years) of areas surrounding the mines

In the study region, some forest compartments (Table.7.3) have very high FHR in present as well as in future too.

Table 7.3: Identification of very high forest health risk compartments in study area

Sasangda forest range compartments IDs		
A-23	KP-4	KP-25
K-1	KP-12	KP-28
G-22	KP-13	KP-27
G-24	KP-14	KP-30
G-25	KP-16	KP-31
G-26	KP-17	KP-33
G-28	KP-23	KP-34
G-23	KP-24	TK-47

7.7.3 Identification of sensitive factors

Twenty-two forests health-related causative factors of present and six of predicted were used for sensitivity analysis. Table 7.4 shows the sensitivity analysis results of the causative factors. In the study area, the highly sensitive factors that affect the FHR most include temperature, drought, wind speed, altitude, slope, deforestation, plant

diversity LST, hot spot, foliar dust concentration, distance from mines, roads, and settlements.

Table. 7.4: Sensitivity analysis results of all forest health causative parameters

i	Features	Very low risk	Low risk	Moderate risk	High risk	Very high risk
1	Temperature (°C)	+2.03	-0.62	+2.69	-1.48	+2.39
2	Rainfall (mm)	+1.87	-1.25	+1.31	-1.64	-0.29
3	Wind speed (m/s) (WS)	-1.89	-2.10	+3.55	+0.52	-0.08
4	Drought	+2.37	-1.59	-1.12	+0.37	-0.04
5	Soil	-1.54	-1.77	+1.87	+1.66	-0.22
6	Lithology	+1.38	-0.11	+0.34	-1.66	+0.06
7	Geomorphology	+1.06	+0.95	+0.67	-1.41	-0.28
8	LULC	-1.02	+0.80	+1.42	-0.90	-0.29
9	Forest health	+0.03	+0.38	+1.20	-1.21	-0.39
10	Forest density	+1.08	-1.43	+1.93	+0.02	+0.40
11	Plant diversity	-1.49	-1.34	+3.90	-0.76	-0.31
12	Tree species	+0.84	-1.65	+1.12	-0.38	+0.72
13	NDVI	-0.67	-0.85	+1.81	-1.86	-0.43
14	Deforestation	+2.76	+3.03	+0.47	-5.03	-1.22
15	Slope °	+1.03	+0.50	-2.21	-0.17	-0.15
16	Altitude (m)	+2.85	+1.91	-1.07	-5.40	-0.28
17	LST (°C)	-0.73	-0.62	+5.68	-3.60	-0.74
18	Hot spot	+1.19	+0.11	+1.92	-2.79	-0.43
19	Foliar dust (g/m ²)	+0.91	+0.46	+1.20	-2.50	-2.02
20	Distance from mines	+1.61	-2.97	+0.75	-2.38	-1.01
21	Distance from roads	+1.65	+2.22	-0.71	-2.56	+0.40
22	Distance from settlements	-1.87	+0.58	+2.10	-0.72	-0.09

Bold values indicate significant results

7.7.4 Correlation of sensitive factors

The Person correlation matrix of FHR and sensitive factors are shown Table.7.5. In most cases, the relationships are showing positive results. The results show that some causative parameters (temperature, wind speed, slope, drought, deforestation, LST, hot spot, foliar dust concentration, distance from mines, roads, and settlements) are a high positive correlation with FHR. The FHR and sensitive factor's pixel values have been calculated based on sixty field sample points (Appendix.5).

Table 7.5. Person correlation matrix of sensitive parameters with FHR

Pearson Correlation	FHR	DM	D	FD	LST	T	DF	PD	HS	S	WS	DR	DS	A
FHR	1	.33	.16	-.32	-.24	.28	.16	.23	.42	.19	.14	.16	.30	.30
DM	.33	1	.55	-.28	-.39	-.21	.20	-.13	.23	-.43	-.34	.28	-.19	.16
D	.26	.55	1	-.21	-.19	-.30	.23	-.23	.15	-.64	-.25	.12	-.50	.26
FD	-.22	-.20	-.21	1	.28	-.27	.22	.25	-.14	.82	.23	-.22	-.24	-.17
LST	-.04	-.09	-.19	.28	1	.31	.37	.23	.18	.32	-.17	.17	.17	.33
T	.28	-.31	-.30	-.17	.31	1	.27	-.21	.50	.28	-.69	.77	.27	.46
DF	.16	.10	.23	.32	.27	.47	1	-.21	.23	-.22	-.16	.13	-.14	.23
PD	.33	-.23	-.23	.25	.33	-.31	-.21	1	-.20	.21	.20	-.16	-.14	-.15
HS	.42	.23	.25	-.14	.18	.50	.23	-.20	1	-.22	-.48	.60	.16	.53
S	.39	-.43	-.64	.18	.13	.22	-.32	.11	-.22	1	.22	-.19	.29	-.22
WS	.24	-.34	-.25	.23	-.37	-.69	-.36	.20	-.48	.22	1	-.89	.11	-.45
DR	.12	.28	.22	-.22	.27	.77	.23	-.16	.60	-.09	-.89	1	.22	.49
DS	.30	-.21	-.50	-.24	.33	.27	-.24	-.24	.36	.29	.21	.12	1	.20
A	.30	.16	.26	-.17	.23	.46	.23	-.15	.53	-.22	-.45	.49	.10	1

(N=60) FHR- Forest health risk, DM Distance from mines, D-Drought, FD- Foliar dust ,LST- Land surface temperature, T- Temperature, DF- Deforestation ,PD- Plant diversity, HS- Hot spot, WS- Wind speed , DR- Distance from roads, DS – Distance from settlements , A- Altitude

7.7.5 Comparison and validation

The FHR present result is validated by sixty field locations of healthy, moderate health, and unhealthy trees (Appendix.6). The ROC curve of the present and predicted is shown in Fig.7.5. The AUC value of FHR for the years present and predicted is 0.76, 0.72, and 0.68.

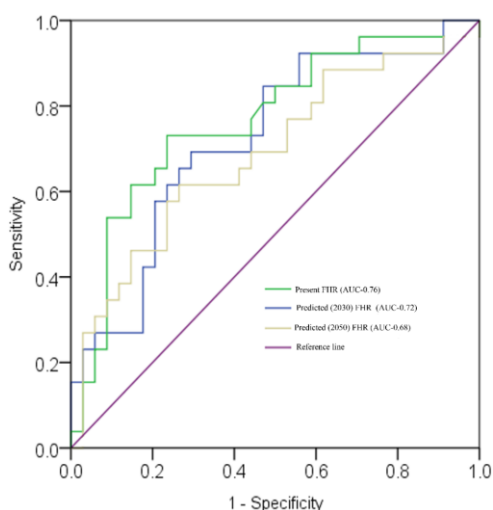


Figure.7.5: ROC Curve for FHR results comparison (Present and predicted years)

The FHR normalized data (Appendix.7) for the years present and predicted are shown in a scatter matrix plot (Fig.7.6). The scatter matrix result shows that the correlation and RMSE values between the years present and predicted (2030) are 0.55 (R^2) and 0.011 (RMSE), respectively. Between the predicted years (2030 & 2050), it is 0.49 (R^2) and RMSE (0.015), and between the years present and predicted (2050), it is 0.33(R^2) and 0.017(RMSE), respectively.

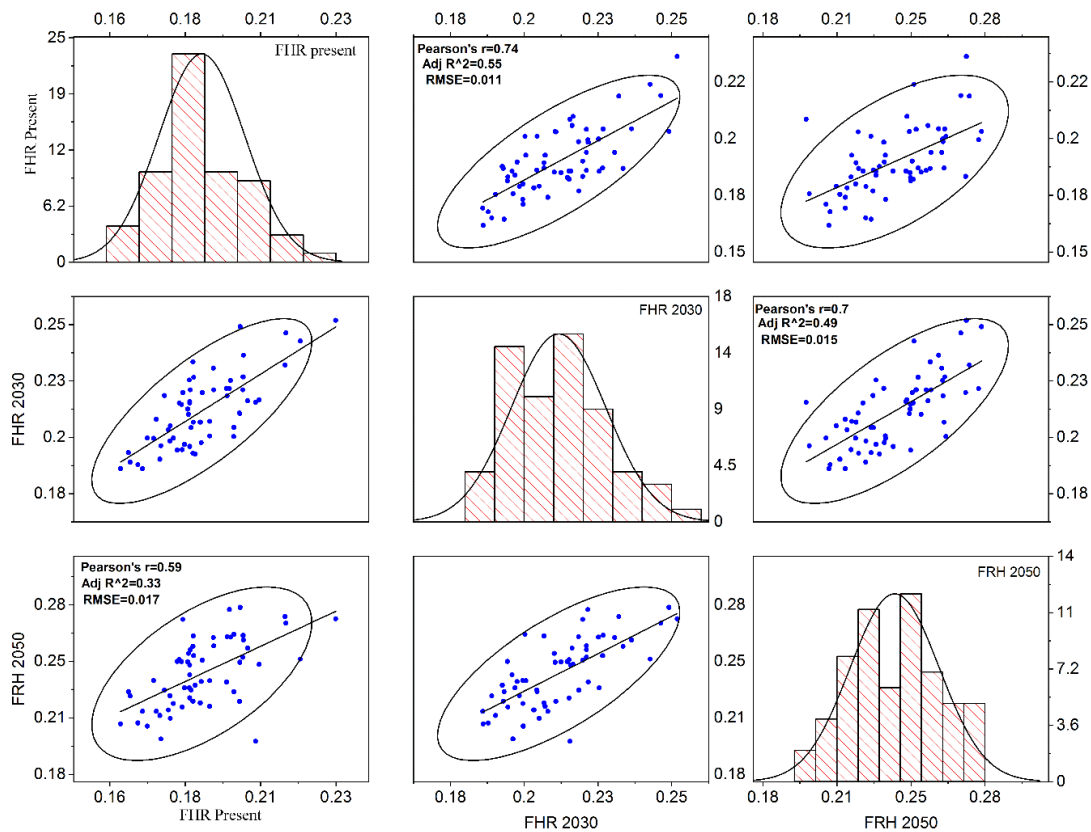


Figure.7.6: Scatter matrix plot of FHR(Present and predicted years)

7.7.6 Relationship between forest health risk, distances from mines with foliar dust concentration

Fig.7.7 has shown the relationship between forest health risk and distance from two mines (Meghataburu and Kiriburu) with foliar dust concentration. It indicated an inverse (negative) relationship between the FHR index and distance from mines with foliar dust concentration. We have also observed a clear negative correlation between mines and forest health during field survey time.

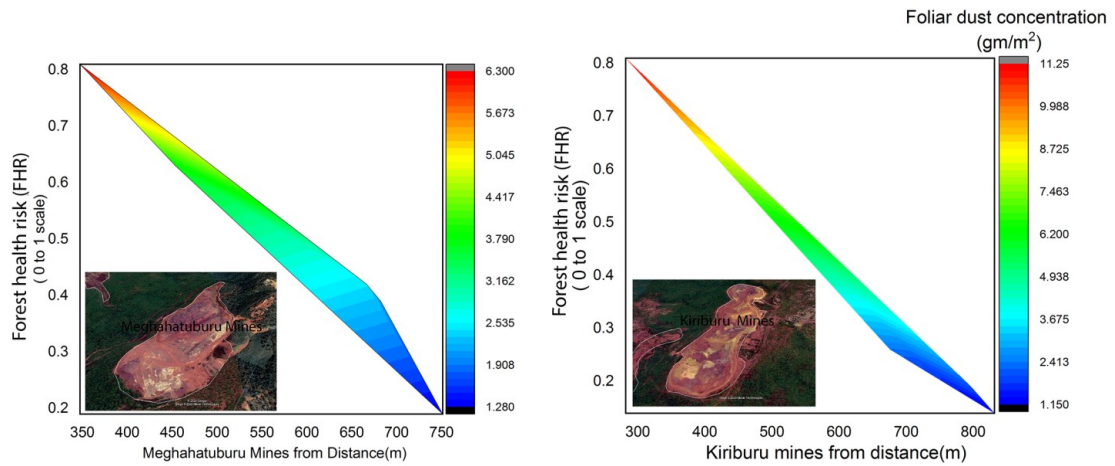


Figure 7.7: Relationship between forest health risk, distances from mines with foliar dust concentration

7.7.7 Discussion

The forest health risk is one of the significant environmental issues as vast forest cover areas are losing daily. Climate change, increasing mining, agricultural, and tribal people's allied activities are causing forest health risks in the study region. However, in this study, FHR assessment and its future impact are predicted in the mining-affected forest area by AHP model-based multi-criteria analysis in a GIS framework.

In this work, twenty-eight forest health-related climate, natural or geomorphic, forestry, environmental, and anthropogenic factors have been assessed for assessment and prediction of FHR. Some researchers used physical and anthropogenic parameters to assess deforestation and mangrove susceptibility (Saha et al., 2020; Chakraborty et al. 2019). They also showed some causative parameters (temperature, rainfall, wind speed, drought, soil, lithology, geomorphology, LULC, slope, altitude, LST, NDVI, agricultural, distance from mines, road, and settlement) play a significant role in causing forest degradation and deforestation. We have used the AHP model based on the multi-criteria analysis in a GIS platform to assess and predict FHR. Some researchers used multi-criteria based statistical models (frequency ratio (FR), logistic regression (LR), analytic hierarchy process (AHP), and random forest (RF)) in a GIS platform to determine the environmental vulnerability, forest fire risk, and deforestation suitability (Sahoo et al., 2019; Kayet et al., 2018; Sahana et al., 2018). They showed that RF and AHP are of higher accuracy than other models.

In this study, FHR assessment and prediction results show that very high-risk zones are located in some forest compartments in the Saranda forest. These compartments are situated in the surrounding sites of Kiriburu and Meghataburu mines. These reasons behind these increments are mining activities, environmental pollution, climate change, and human interface in the study area. The upper and lower hilly sections of the study area show low health risks because those forest compartments areas are far from the mines and in the dense forest. Some studied forest degradation in the mining-affected forest region (Sonter et al., 2017; Ranjan et al., 2019). They also have shown high susceptibility class in mines, transport, agricultural, and settlement's surrounding sites. In this work, a sensitivity analysis was performed by causative factors of forest health. The results show that some parameters (temperature, LST, hot spot, wind speed, deforestation, foliar dust, drought, altitude, slope, plant diversity, and distance from mines, roads, settlements) are most sensitive in this study area due to climate change, deforestation, mining, and human allied activities. Some authors have studied the sensitivity analysis of mangrove and environmental suitability assessment in India (Sahoo et al., 2019; Chakraborty et al. 2019). They have found that some parameters (max temperature, slope, soil moisture, LULC, soil salinity, wind speed, agricultural transportation, and population, activates) are susceptible to mangrove and environmental suitability assessment.

This study used sensitive factors that directly or indirectly affect forest health. The correlation results between FHR and the most sensitive factors show most of the factors are a positive relationship with FHR. Tuominen et al., (2009) and Kayet et al., (2019) worked on forest health in mining-affected forest regions. They showed most of the sensitive parameters are a clear inverse relationship with forest health risk. The study has been shown that validation and comparison of AHP model-based FHR results using the ROC curve. An AUC value (0.76) indicates that present result validation accuracy is perfectly matched with the field obtained locations. Some researchers have used the ROC curve to validate their results of forest fire risk and deforestation susceptibility (Ljubomir et al., 2019; Sahana et al., 2018). They showed of AUC values 0.86 (forest fire) and 0.79 (deforestation susceptibility). For the comparison of three FHR data sets, we used a scatter matrix plot. The correlation result shows that moderately strong relationship (R^2 -0.55 and RMSE-0.011) between the present and predicted (2030) years. Between the two predicted years (2030 &

2050), it is a low, moderate relationship (R^2 -0.49 and RMSE-0.0151), and the years of present and predicted (2050), it is a low relationship (R^2 -0.33 and RMSE-0.017) due to longer time span. Evangelista et al. (2011) worked on forest vulnerability and potential distribution based on present and predicted climate conditions for 2020 and 2050. They had shown a low, moderate relationship between 2020 and 2050 year's results. This study has shown a negative co-relationship between forest health risk and the distance from mines with foliar dust concentration. Some researchers also showed a negative co-relationship between forest health and distance from mines with dust concentration (Tuominen et al., 2009; Kayet et al., 2019).

In this work, some errors have come from the following sources: (1) the inherent errors in acquiring the Hyperspectral and multispectral data have created some noise, and also, the atmospheric errors affected the result. (2) All satellite data used here are of medium spatial resolution (30m), so a problem of mixed pixels also induces error on the end results. (3) The multi-criterion method is entirely based on the weight assignment, so it may also induce some error. (4) The study area is located in the hilly and dense forest region, so shadow and canopy effect errors are obvious. However, we have developed a spatial framework methodology for the assessment and prediction of FHR using the AHP model at Kiriburu and Meghataburu mining-affected forest region. This research work is framed by considering geo-environmental planning and management of the mining-affected forest region. This work is a significant step for protecting forest health, biodiversity conservation, and effective management of the forest.

7.8 Summary

Forest health risk assessment and its prediction are essential for forest planning and management to aid in forest policy. In this study, a total of twenty-eight (twenty-two present and six predicted) causative factors are coupled with multi-criteria based AHP model in a GIS framework for FHR assessment and prediction at Kiriburu, and Meghataburu mining-affected forest region. The result shows that the mining area will increase in the future as well as with a corresponding increase in the risk to forest health due to the mining and allied activities. The assessment results also portrayed that most of the very-high FHR class is close to mining sites. Very high FHR zones are situated at the Kiriburu, and Meghataburu mining surrounding forest

compartments (KP-14, KP-33, KP-32, KP-34, KP-23, KP-24, and KP-31). Predicted FHR (2050) results also show that, these compartments are at high risk.